AIMS Biophysics, 3(4): 596-608.
DOI: 10.3934/biophy.2016.4.596
Received: 01 October 2016
Accepted: 28 November 2016
Published: 02 December 2016

http://www.aimspress.com/journal/biophysics

Research article

A compact and low cost microfluidic cell impedance detection system

Zhe Mei [1,2,*], Zhiwen Liu [1] and Zhiguo Zhou [1]

[1] School of Information and Electronics, Beijing Institute of Technology, Beijing 100081, China
[2] Department of Electrical and Computer Engineering, University of California at San Diego, La Jolla, California 92093-0407, USA

*** Correspondence:** Email: zhemeiucsd@gmail.com; Tel: +8588882520.

Abstract: A microfluidic cell impedance measurement device is presented in this article. The design is simple to fabricate, compact, highly sensitive, and can be easily incorporated into a microfluidic flow cytometer suitable for point-of-care applications. The simple fabrication process and enhanced sensitivity are attributed partly to a novel design of using fluidic channels as "liquid electrodes" to assure a uniform electric field distribution over the cell detection zone. The system's low cost and compact size is due to its sheathless flow design and single circuit board for cell impedance detection, eliminating expensive and bulky equipments such as lock-in amplifiers and additional sheath flow pumps. The device clearly detects and distinguishes polystyrene beads of 7.66 μm, 10.5 μm and 14.7 μm diameters in a mixture with coefficients of variation of 13.87%, 7.98% and 3.74%, respectively. By extracting the features of cell impedance signals using signal processing, we have introduced a new parameter, impedance ratio, to enhance the cell classification capabilities of the device, as demonstrated in the experiment of lymphocytes and granulocytes detection from whole blood.

Keyword: microfluidics; cell impedance detection; cell classification; low cost; impedance ratio

1. Introduction

As a widely used apparatus, Coulter counter detects the electrical impedance signals to count biological cells and measure their sizes in suspension [1]. Counting the populations of certain cell types in fluid such as blood produces important information about individual's health. For example, the counts of neutrophil and monocyte are associated with phagocytosis which constitutes the main

immune function of pathogens removal [2]. For cancer patients undergoing chemotherapy, close monitoring of leukocyte number is important to detect neutropenia. However, the current Coulter counters are too large, expensive and sophisticated for point-of-care clinics and self-administrated test in patient's residence. As a platform technology for health and medicine, microfluidics offers a promising solution for this problem because a microfluidic lab-on-a-chip device can result in significant cost saving, size reduction, and user friendliness [3–5], all being important features for a point-of-care and home care device.

A conventional Coulter counter senses the direct current (DC) change induced by non-conducted particles passing the space between two electrodes. The cell impedance can be derived from this current change. Although the DC cell impedance measurement can be done easily, the applied DC voltage breaks water and generates gas bubbles that interfere with the impedance measurement and introduce noise. For conventional desktop Coulter counters, the gas bubbles may find their way to leave the test area in a proper design [6], but removing gas bubbles has become a significant challenge for microfluidic Coulter counters. Some approaches, including adjustment of the electrode positions [7], increasing the electrode areas [8,9], and using special Ag/AgCl electrodes [10,11], have been investigated to address this issue. However, these methods often complicate the fabrication process substantially and limit the electrode lifetime, which have become serious concerns especially for microfluidic Coulter counters. As a result, alternating current (AC) impedance measurement that does not produce gas bubbles gained its popularity recently. In addition, there have been reports that the AC impedance signals can reveal the internal properties of cells, offering possibilities for discriminating different cell types as a promising scheme for label-free cell detection [12–14].

For the above reasons, much work has been performed to measure AC impedance of cells [15], but so far few devices have demonstrated their viability for point-of-care or self-administered tests. Gawad et al [16] proposed a coplanar microelectrode design to differentiate colloidal beads and also erythrocytes from ghost cells (i.e. solution-filled membrane sacks from lysed RBCs in hypotonic buffer). Wood et al [17] applied a similar design to achieve high throughput counting up to 25000/s using a radio frequency resonance detection technique. However, due to the highly non-uniform electric field distribution over the detection area caused by the geometry of the electrodes, the measured amplitude of impedance varies widely even for the same cell type. The accuracy and reliability of cell differentiation cannot be attained unless the device can produce impedance signals with small coefficients of variation (CVs). To improve the performance, designs including flow focusing features [18] and parallel facing electrodes [14,19,20] (i.e. electrodes on two opposite planes of the channel) were demonstrated. However, the former approach requires sheath flow that considerably complicates the hardware and operation of the system. The latter approach requires special and sophisticated fabrication process, making the device too costly to be disposable.

In this work, we demonstrate a microfluidic Coulter counter with a unique electrode design and an integrated AC impedance circuit to form a highly compact system. We use electrolyte-filled micro channels that intersect the detection area to create a uniform electric field distribution in favor of low CV cell impedance signals. The micro channel electrodes are interfaced with the outside world via direct contacts with two off-the-shelf gold-plated pins sealed to the micro chambers [10,21–24] (Figure 1). The design has greatly simplified the device fabrication process with improved reliability

and reproducibility, saving the lithography, alignment, and metal deposition steps of forming gold electrodes. Furthermore, it creates a much more uniform electric field over the sensing area than the conventional designs, owing to the geometry of the fluidic channels crossing the main channel. Besides the electrode design and fabrication, a low cost AC impedance detection circuit has been developed. Experimental results with three different sizes of polystyrene beads and leukocytes are reported to demonstrate the key functionality. By comparing the results between our device and a commercial flow cytometer, we characterize the device performance and demonstrate its potential for a low-cost point-of-care device for leukocytes counting, among other possible applications.

2. Materials and Methods

2.1. Device design and fabrication

Figure 1 depicts the schematic of our device design. The straight microfluidic channel is 3.5 cm long and has a cross-section of 30 μm × 30 μm (width × height) so that blood cells can travel through without clogging. Two circular chambers with 1mm diameter each are formed on the opposite sides of the microfluidic channel as the liquid electrodes. The liquid electrodes have a 30 μm wide opening to the main channel. To better confine the electric field, a 20 μm long section is introduced between the circular electrode chamber and the microfluidic channel. We use off-the-shelf gold-plated pins (no further treatment required) to interface the liquid electrodes with the outside environment, as shown in Figure 1. Inlet and outlet arrows indicate the flow direction. The distance between the inlet and the detection zone is 1.75 cm.

The microfluidic channel was photolithographically defined by negative photoresist SU8-2015 (Microchem Inc, Newton, MA) on a silicon wafer. The channel patterns were transferred to a PDMS (polydimethylsiloxane, Sylgard 184, Dow Corning) layer following the standard soft lithography process [25]. Through holes were formed on the PDMS layer to create inlet, outlet and electrode chambers, and the PDMS layer was bonded to a glass slide after a UV Ozone treatment. Two gold-plated pins were inserted into the electrode chambers and sealed by PDMS. The device was left in a 60-degree Celsius oven overnight to attain good bonding strength. The device fabrication process is extremely simple and can be easily transferred to hot embossing or injection molding process for high volume production at very low cost.

2.2. Device simulation

To simulate the performance of our design, we performed finite element analysis (COMSOL Multiphysics) to compute the electric field distribution (AC-DC Module, Electric Impedance Sensor Model), flow velocity profile (CFD Module), and impedance signal of a particle passing through the sensing area. One electrode was connected to a current source and the other electrode to the ground. The PDMS and glass were treated as insulators. The 1 × PBS (phosphate buffered saline) buffer was assumed to have its conductivity and relative permittivity: $\sigma = 1.6 S/m, \varepsilon_r = 80$.

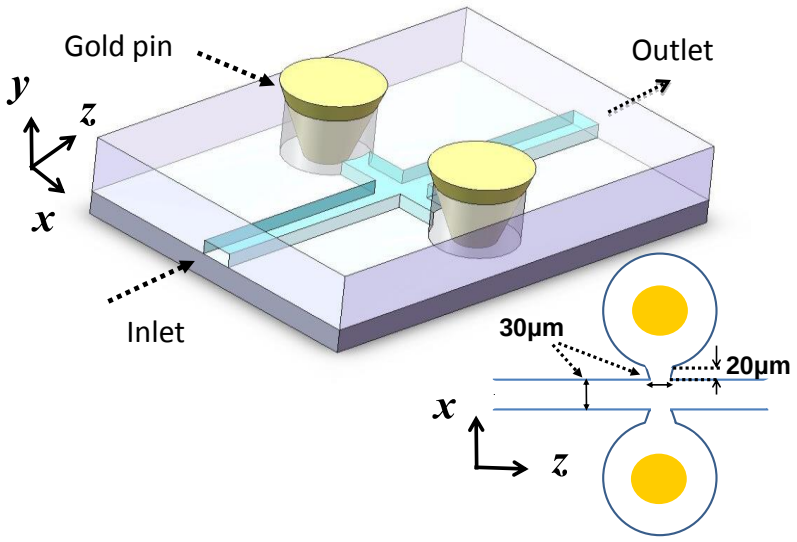

Figure 1. The schematic of device design. Top left: The 3D view of the device. Bottom right: The top view of the device. The dimension of main channel is 30 μm × 30 μm (Width × Height). The opening of sensing area is also 30 μm. Two gold pins are inserted and sealed to both microfluidic electrode chambers.

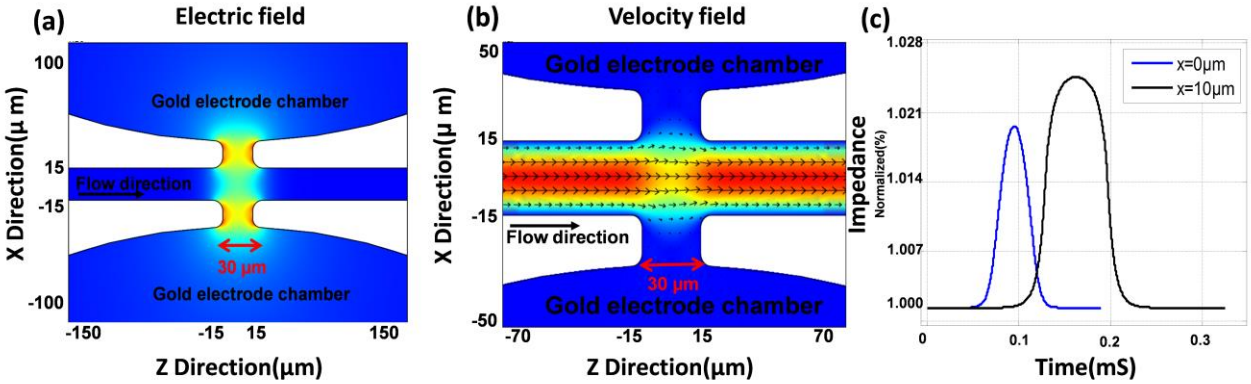

Figure 2. (a) The electric field distribution across the sensing area over the x-z plane. The magnitude of the E-field is represented by color, with red being the strongest field intensity and blue being the lowest. (b) The velocity distribution around the sensing area. The arrows indicate the direction and magnitude of the flow velocity, and the flow speed is also represented by color, with red being the highest speed and blue the lowest. (c) The normalized impedance signals of 10 μm diameter particles passing the sensing area from two different paths: the center of the channel at x = 0 μm (blue curve) and 10 μm from the center (black).

Because the electrode chamber has the same height as the main microfluidic channel and the conductance of the electrolytes (e.g. PBS, serum) is much greater than the surrounding materials (e.g. PDMS and glass), the electric field along the channel height (y-axis) is highly uniform and the simulated impedance signal is invariant to the particle position in the y-axis. On the other hand, there exists some non-uniformity in the electric field along the channel width (x-axis). Since the channel width (x-axis) of sensing area (30 μm) is only a tiny portion of spacing between two electrodes (1 mm), the extent of non-uniformity (electric field gradient) is orders of magnitude less than conventional designs with planar electrodes. Figure 2a shows the field intensity profile in the x-z plane of our design. The velocity profile is also displayed in Figure 2b, indicating the small bending of streamline when the particle is not at the center of the channel. As a result, particles flowing away from the center of the channel produce broader impedance signal which is shown into Figure 2c. Also, the impedance value is normalized to 1 if there is no particle passing through. The 10 μm bead which flows 10 μm away from channel center only has 0.5%–0.6% difference at amplitude with the same bead flowing along with central streamline. The simulation results also produce insight of the achievable coefficients of variation (CVs) of the design. The analyses have shown that our design attains significant improvements over conventional designs with planar electrodes. Also with a simple 2D flow confinement in the x-axis, our design can produce extremely uniform impedance signals since the design requires no flow confinement in the y-direction due to its perfectly uniform E-field distribution along the y-axis. This feature is especially attractive when the device is integrated with microfluidic flow cytometers that usually offers flow confinement in the x-axis but not in the y-axis. Meanwhile, taking advantage of the correlation between the height and width of the cell impedance signal, one can minimize the effects of amplitude variations caused by cell positions in the microfluidic channel further and increase the device performance for cell classification. In the next section, we will discuss a new technique of using "impedance ratio" as a measure of the width of the impedance signal that can assist detection of different cell types.

2.3. Impedance detection circuit

The intensity of impedance signal in a Coulter counter is proportional to the volume ratio between the particle and the volume of the sensing zone. Since the particle volume is usually much smaller than the sensing zone (typically in the order of 1%) in a high-throughput design without the problem of channel clogging, the impedance signal of the particle tends to be weak and noisy. To achieve high sensitivity, people have used synchronous demodulation and lock-in amplifiers to extract impedance signals from the excitation AC signal [12,19,20,26]. Although these approaches improve the detection sensitivity, the system becomes bulky and expensive, and less attractive to point-of-care applications. Here we present a simple, low cost demodulation circuit based on the envelope detection technique. Figure 3 shows the functional block diagram of the AC impedance detection circuit.

The excitation frequency for cell impedance detection ranges from 500 kHz to a few MHz [15]. Here, an excitation signal (Sine wave at 5 volts, 800 KHz) is applied to the electrodes in Figure 1. A current change happen when the particles pass through the sensing zone. A current-to-voltage (I-V) converter transform the current signal into a voltage signal. Then a rectifier with a time constant of

10^{-5} sec (R = 10 Kohm, C = 1nF) is used to detect the envelope of voltage signal. A high-pass filter (338 Hz cutoff frequency) is connected to the output of the rectifier to remove any DC component. Afterwards the signal is amplified by 50 times and go through a low-pass filter (41 KHz cutoff frequency) to remove the AC carrier. Finally, the demodulated signal is amplified again and recorded by a commercial data acquisition board (DAQ USB-6251, National Instrument, Austin, TX, USA) using off-the-shelf software (Signal Express 2010, National Instrument, Austin, TX, USA). The sampling rate of the DAQ is set at 200 k/s. All data are processed by a custom signal processing algorithm implemented in Matlab.

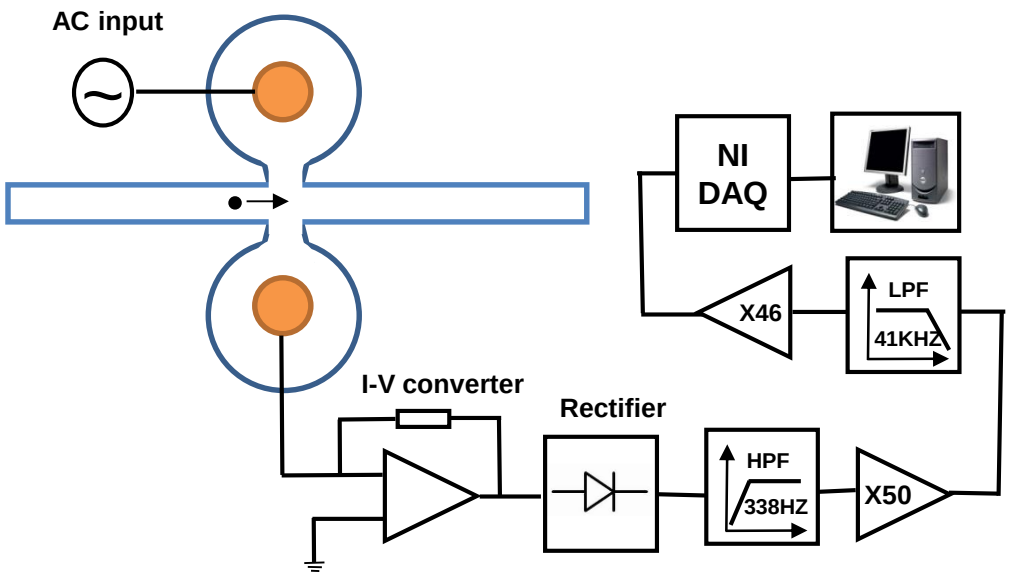

Figure 3. Diagram of impedance detection circuit for microfluidic Coulter counter. HPF and LPF stand for high pass filter and low pass filter, respectively.

2.4. Sample preparation

Two sets of sample were used in our test: polystyrene beads in PBS and leukocytes from whole blood. We mixed polystyrene beads with diameters of 7.66 μm, 10.5 μm and 14.7 Hz (PPS-6K, Spherotech, Lake forest, IL, USA) in the sample. The beads were spiked in 1 × PBS containing 12% sucrose to achieve gravity neutral suspension. Each sample was sonicated for at least three minutes before being introduced to the device. The initial concentration was around 150 beads/μL. Leukocyte samples were obtained from whole blood purchased from a local blood bank and prepared according to a common procedure involving lysing red blood cells, centrifuging, extracting supernatant, and diluting the supernatant with 1 × PBS buffer. We repeated the above process twice to obtain leukocyte samples with higher purity.

3. Results and Discussions

3.1. Polystyrene particle counting

The performance of this device was first examined by mixed polystyrene beads of three different sizes: 7.66 μm, 10.5 μm and 14.7 Hz. Figure 4a shows the raw data of the bead mixture directly from the output of the circuit in Figure 3, recorded over a period of 8 seconds. Each peak indicates one particle passing through the sensing area. A custom peak detection algorithm implemented in Matlab was used to identify the impedance signal. Figure 4b shows typical signal waveforms of the beads. From left to right, three signals indicate 7.66 μm, 10.5 μm and 14.7 Hz beads, respectively. It should be noticed that if two beads pass the sensing area simultaneously, the impedance signal amplitude will increase. To achieve better performance, the initial sample concentration can not be too high. Also, the proper sample preparation such as vortex is strongly recommended.

One notable feature in Figure 4 is the negative tail of signal. In principle, a passing particle decreases the current density of the sensing area and produces a dip in the voltage signal, which is subsequently converted into the impedance signal. In our circuit, we use an inverting amplifier to change the polarity of the impedance signal from a dip to a positive peak. However, the high pass filter behind the I-V converter has differential effects on the signal. By setting the cutoff frequency of the high pass filter at 338 Hz (or any frequency around 300 Hz), we can intentionally produce a negative tail following the positive peak, as a signature for a true impedance signal. This feature helps the algorithm to register the real events from noise, which is especially useful when the signal-to-noise ratio is low. The negative tail will go away when the high pass filter cutoff frequency reduce to a few hertz.

Figure 4c is a close-up view for a single event. At a flow rate of 30 L/min, the average transit time of each particle across the detection zone is less than 1ms, which enables a throughput of over 1000 particles/second. The system can be operated at higher throughput by increasing the flow rate or tweaking the detection circuits, such as adjusting the time constant of rectifier.

During experiment, samples were collected at the outlet reservoir and tested by a commercial flow cytometer (Accuri C6, Becton & Dickinson, Ann Arbor MI, USA) for comparison. Figure 5a shows the scattering plot of the bead mixture based on the intensities of optical forward scattering (FSC) and side scattering (SSC) signals. The gating regimes and the relative percentage of each type of bead in the mixture are also indicated in the plot. The histogram of the impedance signal from our device is shown in Figure 5b. Three distinct populations corresponding to three sizes of beads are clearly distinguishable from both the commercial flow cytometer and our device, although our device is expected to cost less than 10% of a flow cytometer.

The simulation results in section 2.2 show that, besides the amplitude difference, beads at different positions also have different signal widths. Same sized particles are supposed to show similar impedance waveform if their flow paths in the microfluidic channel are similar to each other. The width of impedance signal will be different if beads have different flow trajectory in the microfluidic channel. The impedance width can act as extra dimension for cell classification. However, it requires high sampling rate ADC to obtain accurate width information due to the narrow sensing area and fast particle velocity. One alternative and easy method to represent the width of the impedance signal is to take the ratio of the signal after two digital filters of different cutoff

frequencies, yielding a quantity defined as "impedance ratio". The selection of cutoff frequencies depends on the geometry of the electric field and flow rate. One of cutoff frequency is set at good value to enhance signal to noise ratio. The other one, we intentionally chose low value to reshape signal waveform. Those beads population has similar width which will produce tight value of impedance ratio. The beads population has wide width distribution will give wide impedance ratio values. Since the cutoff frequencies are chosen digitally, we can adjust their values according to the sample flow rates. At a sampling rate of 200 KHz, we have great flexibilities to choose the cutoff frequencies over all practical flow rates of the microfluidic device. Figure 5c presents a density plot with the amplitude versus the normalized impedance ratio. The cutoff frequencies of digital filter here are set at 5 KHz and 20 KHz, respectively. The result shows that smaller beads have a wider position distribution in the microfluidic channel than larger beads, which is consistent with the result reported in earlier publications [27,28]. The CV and ratios of population for each bead, measured by the commercial flow cytometer and our device, are summarized in Table 1 after gating.

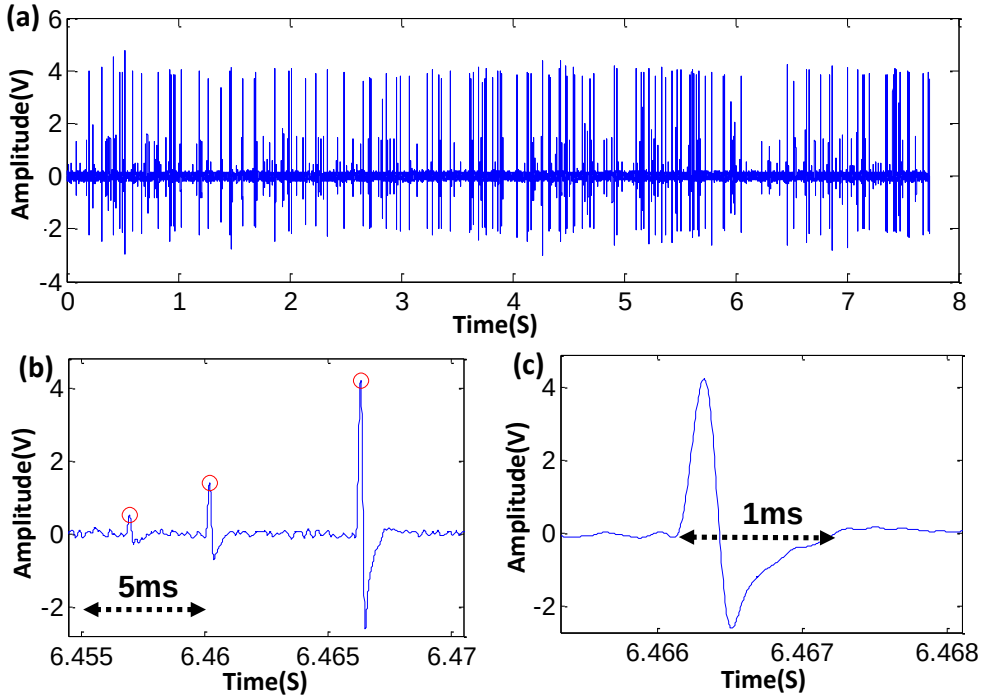

Figure 4. Test results of mixed polystyrene beads (7.66 μm, 10.5 μm and 14.7 Hz) at 800 KHz, 5 V peak-to-peak sinusoidal excitation. (a) Raw data from the circuit in Figure 2. (b) Zoom-in view of three events representing 7.66 μm, 10.5 μm and 14.7 Hz beads from left to right. The red circles indicate the peak positions detected by the peak-detection algorithm. (c) Typical waveform of a single event. The transit time for each event is shorter than 1ms including the negative tail due to the high-pass filter.

The microfluidic Coulter counter registered 15829 events from 174 μL of sample. The results of commercial flow cytometer were produced from 8076 registered events from 120 μL of sample collected at the outlet reservoir of the microfluidic Coulter counter. The counting numbers did not

match since beads were lost during sample transportation, re-collection, and vertex before loading to the commercial flow cytometer. However, the population percentage for three types of beads measured from the commercial system and our device agreed very well. Their numbers also agreed well with the initial sample mixture, which was 1:1:1 for three types of beads. The detailed results are summarized in Table 1.

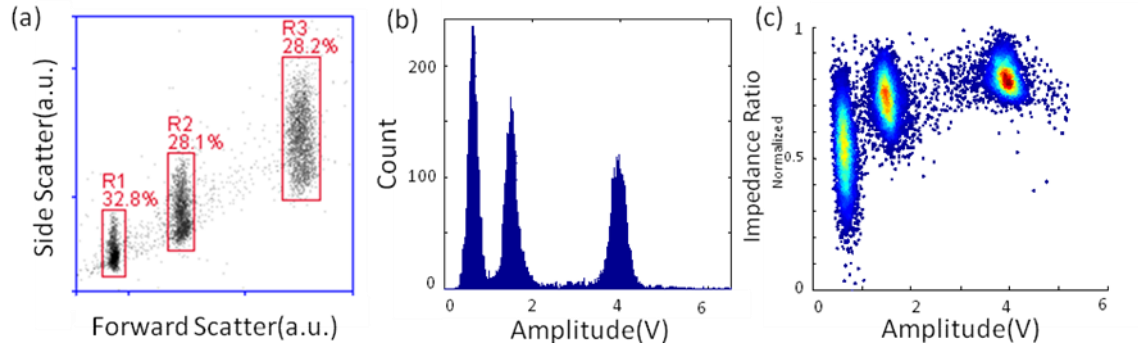

Figure 5. (a) The plot of forward scatter intensity versus side scattering intensity. R1, R2 and R3 indicate bead populations with diameter of 7.66 μm, 10.5 μm and 14.7 Hz, respectively. (b) Histogram produced by the microfluidic Coulter counter. (c) Density plot with normalized impedance ratio versus amplitude produced by the microfluidic Coulter counter. Colors change from blue to red as densities increase.

Concerning CVs, the microfluidic Coulter counter produces CVs of 13.87%, 7.98% and 3.74% for 7.66 μm, 10.5 μm and 14.7 Hz beads, respectively. In comparison, the corresponding CVs from the forward scattering signal of a commercial flow cytometer are 2.75%, 2.77% and 2.50%. As shown in the simulations (Figure 2), although our design eliminates the electric field non-uniformity along the y-axis, the velocity field distribution and fringing field contribute to the dependence of signal amplitude on the bead's position along the x-axis. Considering that no flow confinement is introduced in our device to reduce the system complexity and lower the cost, these results represent a marked improvement compared to existing microfluidic Coulter counters.

Table 1. Coefficients of variation and percentage of population comparison between a commercial cytometer and our microfluidic Coulter counter.

	Commercial flow cytometer		Microfluidic Coulter counter	
	Population percentage	FSC CV	Population percentage	Impedance CV
7.66 μm bead	32.82%	2.75%	33.06%	13.87%
10.5 μm bead	28.09%	2.77%	29.38%	7.98%
14.7 μm bead	28.15%	2.50%	27.22%	3.74%

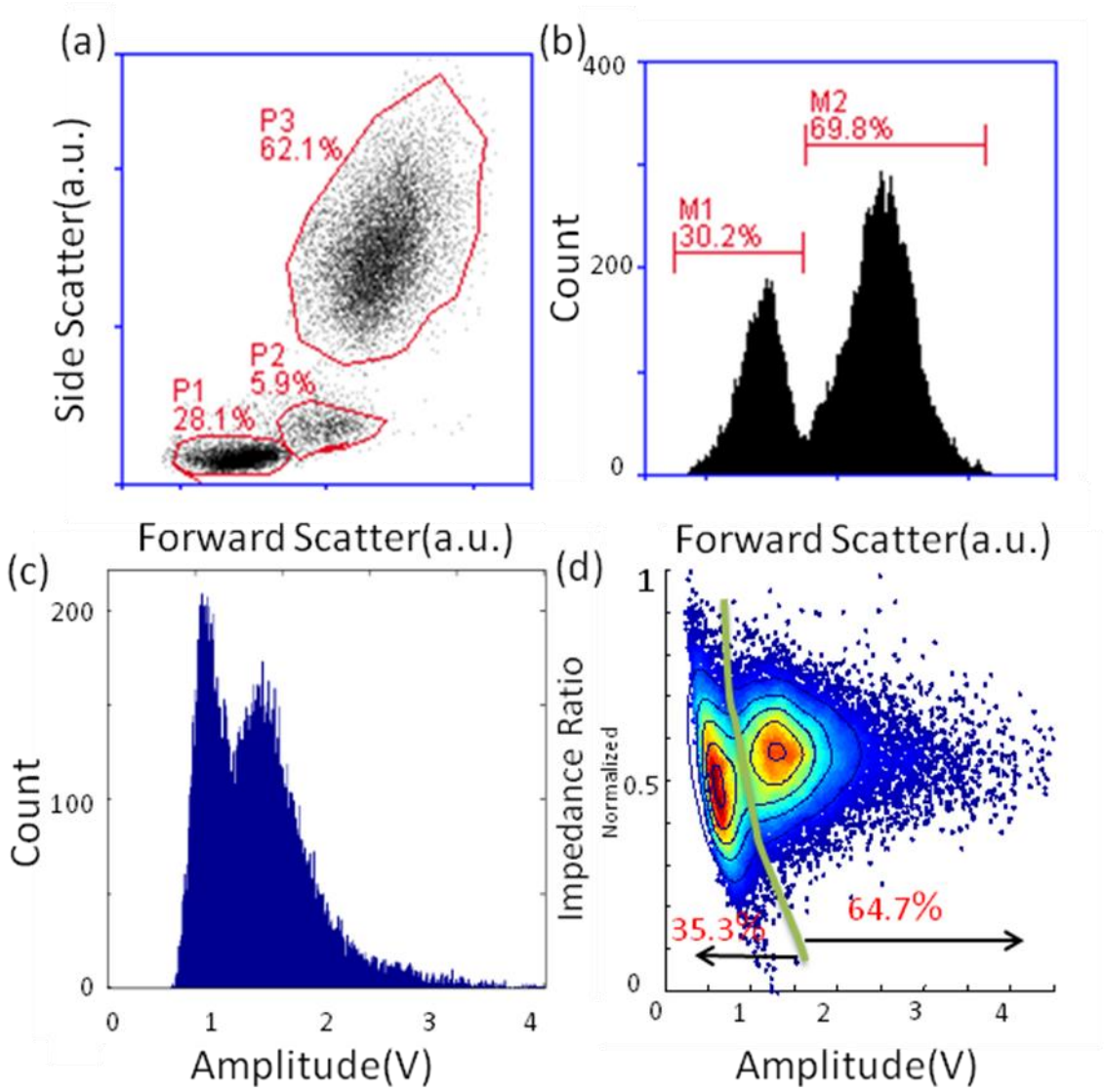

Figure 6. Scatter plot and histogram of WBC sample measured by a commercial cytometer (a,b) and a microfluidic Coulter counter (c). (a) The plot of forward scattering versus side scattering. The three main populations of white blood cells, lymphocytes, monocytes and neutrophils are indicated by P1, P2 and P3, respectively. (b) Histogram from a commercial cytometer. M1 and M2 are the ratios of counting numbers. (c) Histogram from the microfluidic Coulter counter. (d) Density plot with normalized impedance ratio versus amplitude produced by the microfluidic device. Colors change from blue to red as cell densities increase. Black curves are equal-density contours. The green line is the boundary that separate the cells into subpopulations based on extreme points of the contour.

3.2. Leukocytes detection

Leukocytes or white blood cells (WBCs) are critical to immune functions. The overall population of leukocytes and the subpopulation of each leukocyte type provide important health and

disease information. Therefore we used leukocyte samples for preliminary assessment of the prospect of our device for health related applications. After standard blood preparation described in section 2.4, we split the sample into two tubes. One tube contained 200 μL of sample for the commercial flow cytometer, and the other tube contained 600 μL of sample for our device. Again, the results were compared against the gold standard (i.e. flow cytometer). The FSC-SSC scatter plot from a commercial cytometer is shown in Figure 6a, revealing three subpopulations for lymphocytes, monocytes and neutrophils. Figure 6b shows the histogram of counting number based on forward scattering intensity. It shows two populations: 30.2% (M1) and 69.8% (M2). Here M1 is attributed to lymphocytes and M2 is the combined population of monocytes and neutrophils. The histogram based on the microfluidic Coulter counter is plotted in Figure 6c. The result shows two peaks, with lymphocytes having lower amplitude and neutrophils/monocytes having higher amplitude. Because of the significant overlap between these two populations, it is difficult to precisely obtain the population of lymphocytes and neutrophils/monocytes using only one single parameter. Figure 6d shows the density plot of normalized impedance ratio versus amplitude. Smaller cells have a wider position distribution than larger cells, which is in consistence with the behaviors of beads shown in Figure 5. Aided by the impedance ratio as a new parameter, the populations of lymphocytes and granulocytes were much more clearly distinguishable. The density contours and the gating boundary are presented to distinguish two main subpopulations of leucocytes. The cell cluster on the right side of the boundary takes 64.7% of the entire population and the cluster on the left side of the boundary takes 35.3%. This is in agreement with the results from the commercial cytometer that separate WBCs into neutrophils and lymphocytes/monocytes as two main groups (Figure 6b).

4. Conclusion

We demonstrate a compact microfluidic cell impedance detection system that is sensitive, easy to fabricate, and highly cost effective. Compared to conventional devices of the same functions, our system uses a design of “liquid electrodes” to produce a much more uniform electric field distribution, resulting in high sensitivity and low CVs. The system is self-contained with the implementation of an impedance detection circuit. The “liquid electrodes” are microfluidic chambers interfacing the outside environment with inserted gold-plated pins. Our custom designed circuit board detects the AC impedance signal generated by passing beads or cells. The circuit replaces the lock-in amplifiers and complicated electronic instrument used in earlier works, greatly reducing the cost and size of the system and simplifying the operation. Data from polystyrene beads and leukocytes confirm that our device produces decent CVs among microfluidic Coulter counters without any flow confinement, and give promising results of leukocyte detection and classification. Although the results are preliminary, they represent major improvements in microfluidic impedance-based cell analysis devices with attractive cost, size, and functionality as a point-of-care device.

Acknowledgements

We acknowledge the technical support of the staff of the Nano3 (Nanoscience, Nanoengineering, Nanomedicine) Facility in Calit-2 in University of California at San Deigo. We also thank Prof. Yuhwa Lo and Dr. Sunghwan Cho for technical discussions and assistances in preparation of the manuscript. This work was supported by National Natural Science Foundation of China No.61001063.

Conflict of Interest

The authors declare that there is no conflict of interests.

Reference

1. Graham MD (2003) The coulter principle: foundation of an industry. *J Lab Autom* 8: 72–81.
2. Dale DC, Boxer L, Liles WC (2008) The phagocytes: neutrophils and monocytes. *Blood* 112: 935–945.
3. Streets AM, Huang Y (2013) Chip in a lab: Microfluidics for next generation life science research. *Biomicrofluidics* 7: 011302.
4. Watkins N, Irimia D, Toner M, et al. (2011) On a chip. *Ieee Pulse* 2: 19–27.
5. Mark D, Haeberle S, Roth G, et al. (2010) Microfluidic lab-on-a-chip platforms: requirements, characteristics and applications. *Chem Soc Rev* 39: 1153–1182.
6. Miyamura K (2004) Development of blood cell counter for point of care testing (POCT). *Horiba Technical Journal "Readout"*: 56–61.
7. Tanabe R, Hata S, Shimokohbe A (2006) MEMS complete blood count sensors designed to reduce noise from electrolysis gas. *Microelectron Eng* 83: 1646–1650.
8. Zheng S, Liu M, Tai YC (2008) Micro coulter counters with platinum black electroplated electrodes for human blood cell sensing. *Biomed Microdevices* 10: 221–231.
9. Jagtiani AV, Carletta J, Zhe J (2011) An impedimetric approach for accurate particle sizing using a microfluidic Coulter counter. *J Micromech Microeng* 21: 045036.
10. Chun H, Chung TD, Kim HC (2005) Cytometry and velocimetry on a microfluidic chip using polyelectrolytic salt bridges. *Anal Chem* 77: 2490–2495.
11. Joo S, Kim KH, Kim HC, et al. (2010) A portable microfluidic flow cytometer based on simultaneous detection of impedance and fluorescence. *Biosens Bioelectron* 25: 1509–1515.
12. Holmes D, Pettigrew D, Reccius CH, et al. (2009) Leukocyte analysis and differentiation using high speed microfluidic single cell impedance cytometry. *Lab Chip* 9: 2881–2889.
13. Cheung KC, Berardino MD, Schade-Kampmann G, et al. (2010) Microfluidic impedance-based flow cytometry. *Cytometry A* 77: 648–666.
14. Cheung KC, Gawad S, Renaud P (2005) Impedance spectroscopy flow cytometry: on-chip label-free cell differentiation. *Cytometry A* 65: 124–132.
15. Sun T, Morgan H (2010) Single-cell microfluidic impedance cytometry: a review. *Microfluid Nanofluidics* 8: 423–443.

16. Gawad S, Schild L, Renaud P (2001) Micromachined impedance spectroscopy flow cytometer for cell analysis and particle sizing. *Lab Chip* 1: 76–82.
17. Wood Dk, Oh SH, Lee SH, et al. (2005) High-bandwidth radio frequency Coulter counter. *Appl Phys Lett* 87: 184106.
18. Rodriguez-Trujillo R, Castillo-Fernandez O, Garrido M, et al. (2008) High-speed particle detection in a micro-Coulter counter with two-dimensional adjustable aperture. *Biosens Bioelectron* 24: 290–296.
19. Bernabini C, Holmes D, Morgan H (2011) Micro-impedance cytometry for detection and analysis of micron-sized particles and bacteria. *Lab Chip* 11: 407–412.
20. Spencer D, Morgan H (2011) Positional dependence of particles in microfludic impedance cytometry. *Lab Chip* 11: 1234–1239.
21. Lee DW, Yi S, Cho YH (2008) A flow rate independent cell concentration measurement chip using electrical cell counters across a fixed control volume. *J Microelectromech S* 17: 139–146.
22. Jagtiani AV, Sawant R, Zhe J (2006) A label-free high throughput resistive-pulse sensor for simultaneous differentiation and measurement of multiple particle-laden analytes. *J Microelectromech S* 16: 1530.
23. Zhan Y, Cao Z, Bao N, et al. (2012) Low-frequency ac electroporation shows strong frequency dependence and yields comparable transfection results to dc electroporation. *J Control Release* 160: 570–576.
24. Demierre N, Braschler T, Linderholm P, et al. (2007) Characterization and optimization of liquid electrodes for lateral dielectrophoresis. *Lab Chip* 7: 355–365.
25. Friend J, Yeo L (2010) Fabrication of microfluidic devices using polydimethylsiloxane. *Biomicrofluidics* 4: 026502.
26. Van BC, Gwyer JD, Deane S, et al. (2011) Integrated systems for rapid point of care (PoC) blood cell analysis. *Lab Chip* 11: 1249–1255.
27. Wu TF, Mei Z, Pion-Tonachini L, et al. (2011) An optical-coding method to measure particle distribution in microfluidic devices. *AIP Adv* 1: 022155.
28. Mei Z, Wu TF, Pion-Tonachini L, et al. (2011) Applying an optical space-time coding method to enhance light scattering signals in microfluidic devices. *Biomicrofluidics* 5: 034116.

AIMS Press